

The central amygdala controls learning in the lateral amygdala

Kai Yu¹, Sandra Ahrens¹, Xian Zhang¹, Hillary Schiff¹, Charu Ramakrishnan^{2,3}, Lief Fenno^{2,3}, Karl Deisseroth^{2,3}, Fei Zhao⁴, Min-Hua Luo⁴, Ling Gong⁵, Miao He⁵, Pengcheng Zhou⁶, Liam Paninski⁶ & Bo Li^{1*}

Experience-driven synaptic plasticity in the lateral amygdala is thought to underlie the formation of associations between sensory stimuli and an ensuing threat. However, how the central amygdala participates in such a learning process remains unclear. Here we show that PKC- δ -expressing central amygdala neurons are essential for the synaptic plasticity underlying learning in the lateral amygdala, as they convey information about the unconditioned stimulus to lateral amygdala neurons during fear conditioning.

Adaptive behavioral responses to a threat are dependent on memories linking the threat with its associated environmental cues. Extensive evidence indicates that such memories are formed in the lateral amygdala (LA), in which the convergence of information about a neutral environmental cue (also known as the conditioned stimulus or CS) and a threatening event (also known as the unconditioned stimulus or US), as exemplified in Pavlovian auditory fear conditioning (FC) by pairing of a sound with electrical shock, induces Hebbian plasticity¹. This plasticity, expressed as strengthening of the synapses onto LA neurons driven by CS inputs, is considered a cellular substrate of aversive memory¹.

Recent studies demonstrate that the central amygdala (CeA) is another amygdala nucleus indispensable for learning during FC^{2–8}. Nevertheless, how the CeA contributes to the learning process remains unclear. In traditional views, the LA and the CeA are, respectively, the main input and output nuclei of the amygdala, so that information flows from the LA to the CeA^{1,6}. However, direct evidence for such serial information processing in FC has been lacking. On the other hand, previous studies have described functions of the CeA—including its involvement in attention or alerting processes—that are independent of the LA^{9,10}, suggesting that the two nuclei are not simply organized in series.

We reasoned that, if information indeed flows serially from the LA to the CeA, then inhibiting the CeA should leave the FC-induced LA synaptic plasticity intact. To test this hypothesis, we inhibited the major classes of CeA neurons in mice with the tetanus toxin light chain (TeLC), which blocks neurotransmitter release (Methods). We first targeted somatostatin-expressing (SOM⁺) neurons in the lateral CeA (CeL) by bilaterally injecting the CeL of *Som-Cre* mice, in which Cre recombinase is expressed under the endogenous *Som* promoter^{2,4}, with an adeno-associated virus (AAV) expressing

TeLC-GFP or GFP (as a control) in a Cre-dependent manner (Methods and Supplementary Fig. 1a–f). In the auditory thalamus (the medial geniculate nucleus or MGN, which transmits CS information in auditory FC) of the same mice, we also injected an AAV expressing the light-gated cation channel channelrhodopsin (ChR2; Methods and Supplementary Fig. 1a,f).

These mice were subsequently subjected to auditory FC, following which they were killed and acute brain slices were prepared. In LA neurons in these slices, we recorded the AMPA-receptor- and NMDA-receptor-mediated components of synaptic responses evoked by light stimulation of MGN axons (Supplementary Fig. 1a–c). Inhibition of SOM⁺ CeL neurons did not affect the FC-induced synaptic strengthening, measured as an increase in the AMPA/NMDA ratio¹¹, onto LA neurons (Supplementary Fig. 1b,c). This manipulation did, however, cause impairment in conditioned freezing behavior (Supplementary Fig. 1d), an effect consistent with our previous findings^{2,4}.

We next examined the effects of inhibiting protein kinase C- δ -expressing (PKC- δ ⁺) CeL neurons, another major population in the CeL², with the TeLC in *Prkcd-Cre* mice that express Cre in PKC- δ ⁺ CeL neurons¹² (Fig. 1a–d and Supplementary Figs. 2 and 3a–d). To our surprise, inhibiting PKC- δ ⁺ CeL neurons completely abolished the FC-induced synaptic strengthening onto LA neurons (Fig. 1a–c). Notably, unilateral inhibition of PKC- δ ⁺ CeL neurons was sufficient to abolish the synaptic strengthening in the ipsilateral LA, while leaving that in the contralateral LA intact (Fig. 1b,c). Furthermore, bilateral inhibition of PKC- δ ⁺ CeL neurons drastically impaired conditioned freezing (Fig. 1d and Supplementary Figs. 2 and 3a,b), while unilateral inhibition of these neurons was less effective (Supplementary Fig. 3a). Bilateral inhibition of PKC- δ ⁺ CeL neurons also completely abolished conditioned lick-suppression⁷ (Supplementary Fig. 4). Such conditioned suppression of action, like the conditioned freezing, has been shown to depend on both LA plasticity¹¹ and CeL function⁷.

The behavioral effect of PKC- δ ⁺ CeL neuron inhibition is likely caused by impairment in learning rather than expression of the defensive responses, as suggested by the impaired LA synaptic plasticity. To verify this possibility, we used optogenetics. We bilaterally injected the CeL of the *Prkcd-Cre* mice with a Cre-dependent AAV expressing the light-sensitive proton pump archaerhodopsin

¹Cold Spring Harbor Laboratory, Cold Spring Harbor, NY, USA. ²Howard Hughes Medical Institute, Stanford University, Stanford, CA, USA. ³Department of Bioengineering and Department of Psychiatry and Behavioral Sciences, Stanford University, Stanford, CA, USA. ⁴State Key Laboratory of Virology, CAS Center for Excellence in Brain Science and Intelligence Technology (CEBSIT), Wuhan Institute of Virology, Chinese Academy of Sciences, Wuhan, China. ⁵Institutes of Brain Science, State Key Laboratory of Medical Neurobiology, Collaborative Innovation Center for Brain Science, Fudan University, Shanghai, China. ⁶Departments of Statistics and Neuroscience, Center for Theoretical Neuroscience, and Grossman Center for the Statistics of Mind, Columbia University, New York, NY, USA. Sandra Ahrens and Xian Zhang contributed equally to this work. *e-mail: bli@cshl.edu

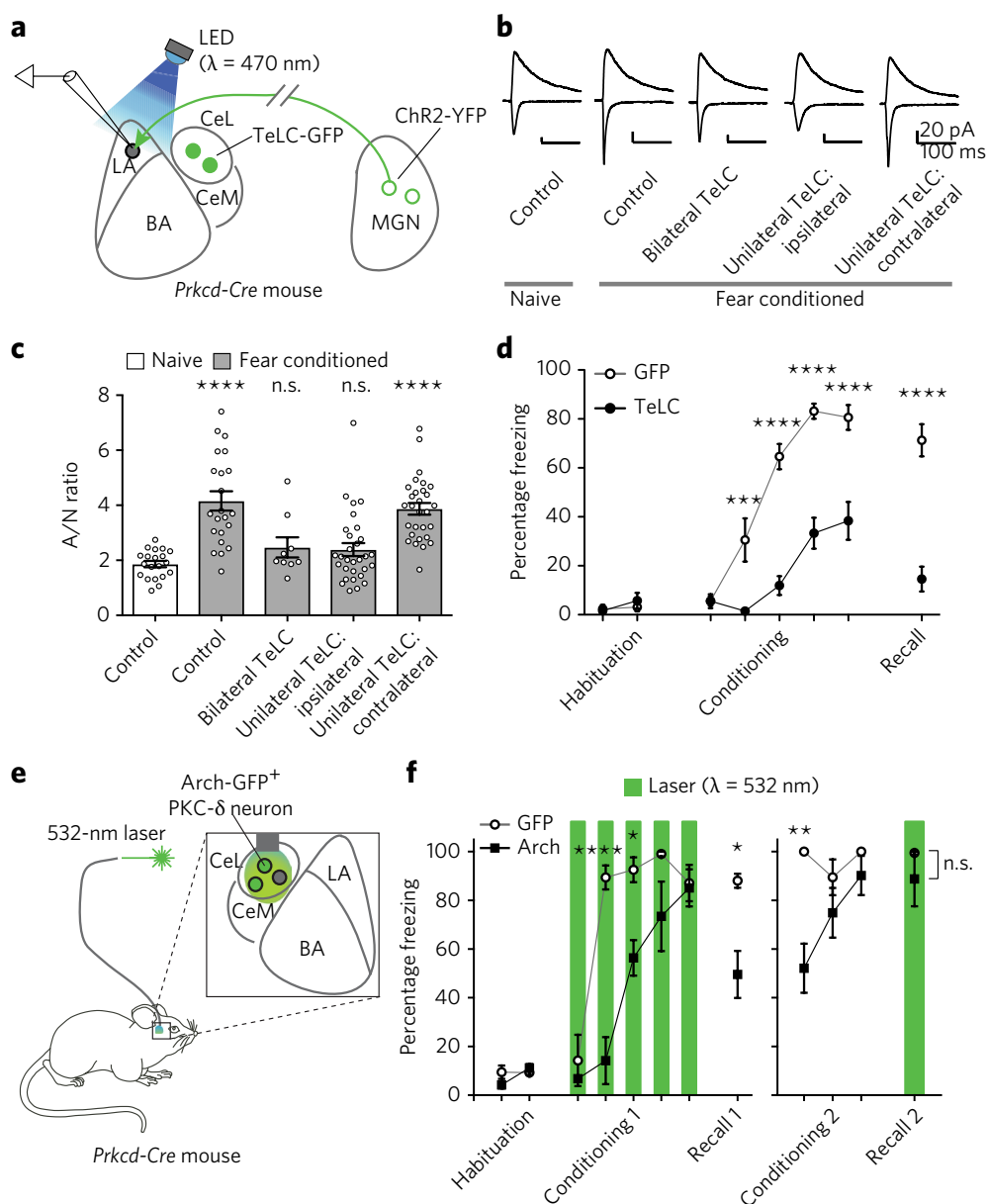


Fig. 1 | PKC- δ^+ CeL neurons are required for the plasticity underlying learning in the LA. **a, A schematic of the experimental configuration. Pyramidal neurons in the dorsal LA were chosen for recording. **b**, Example traces of the excitatory postsynaptic currents (EPSCs). **c**, Quantification of AMPA/NMDA (A/N) ratio (from left to right: $n = 20$ (total) cells from 3 mice, 22 cells from 3 mice, 9 cells from 2 mice, 29 cells from 4 mice, 30 cells from 4 mice; $F_{4,105} = 15.28$, $P < 0.0001$; **** $P < 0.0001$; n.s., not significant ($P > 0.05$), compared with the control and naive control groups; one-way ANOVA followed by Bonferroni's test). **d**, Quantification of freezing behavior (GFP, $n = 11$, TeLC, $n = 11$; $F_{1,20} = 57.88$, $P < 0.0001$; **** $P < 0.0001$, *** $P < 0.001$, two-way repeated-measures (RM) ANOVA followed by Bonferroni's test). **e**, A schematic of the experimental configuration. **f**, Quantification of freezing behavior (GFP, $n = 3$, archaerhodopsin (Arch), $n = 4$; $F_{1,5} = 52.41$, $P < 0.001$; * $P < 0.05$, ** $P < 0.01$, **** $P < 0.0001$; n.s., not significant ($P > 0.05$); two-way RM-ANOVA followed by Bonferroni's test). Note that the light illumination period coincided with the duration of CS and US presentations in each trial. Data are presented as mean \pm s.e.m. in **c**, **d**, and **f**. BA, basal amygdala.**

(see Methods) and subsequently implanted optical fibers above the CeL for light delivery (Fig. 1e and Supplementary Fig. 3e,f). Optogenetic inhibition of PKC- δ^+ CeL neurons during conditioning, but not during memory recall, significantly reduced conditioned freezing behavior (Fig. 1f). Of note, we found that optogenetic inhibition of PKC- δ^+ CeL neurons in naive mice did not induce freezing behavior or other aversive responses (Supplementary Fig. 5). Together, these results indicate that the activity of PKC- δ^+ CeL neurons is required for both the FC-induced LA synaptic plasticity and learning.

Why are neurons in the CeL required for synaptic plasticity and learning in the LA? In auditory FC, the convergence of sound

(CS) and shock (US) onto LA neurons is thought to be a prerequisite for these neurons to undergo synaptic strengthening underlying learning. While sound can reach the LA via the MGN and auditory cortex, the route through which shock is transmitted to the LA remains elusive¹. Notably, it has recently been shown that CeL neurons, including PKC- δ^+ neurons, are the direct postsynaptic targets of the parabrachial nucleus (PBN)¹³, a brainstem structure that provides nociceptive signals, and that activation of the PBN–CeL pathway is sufficient to drive aversive learning^{13,14}. These findings raise the possibility that PKC- δ^+ CeL neurons may participate in relaying US information from the PBN during FC.

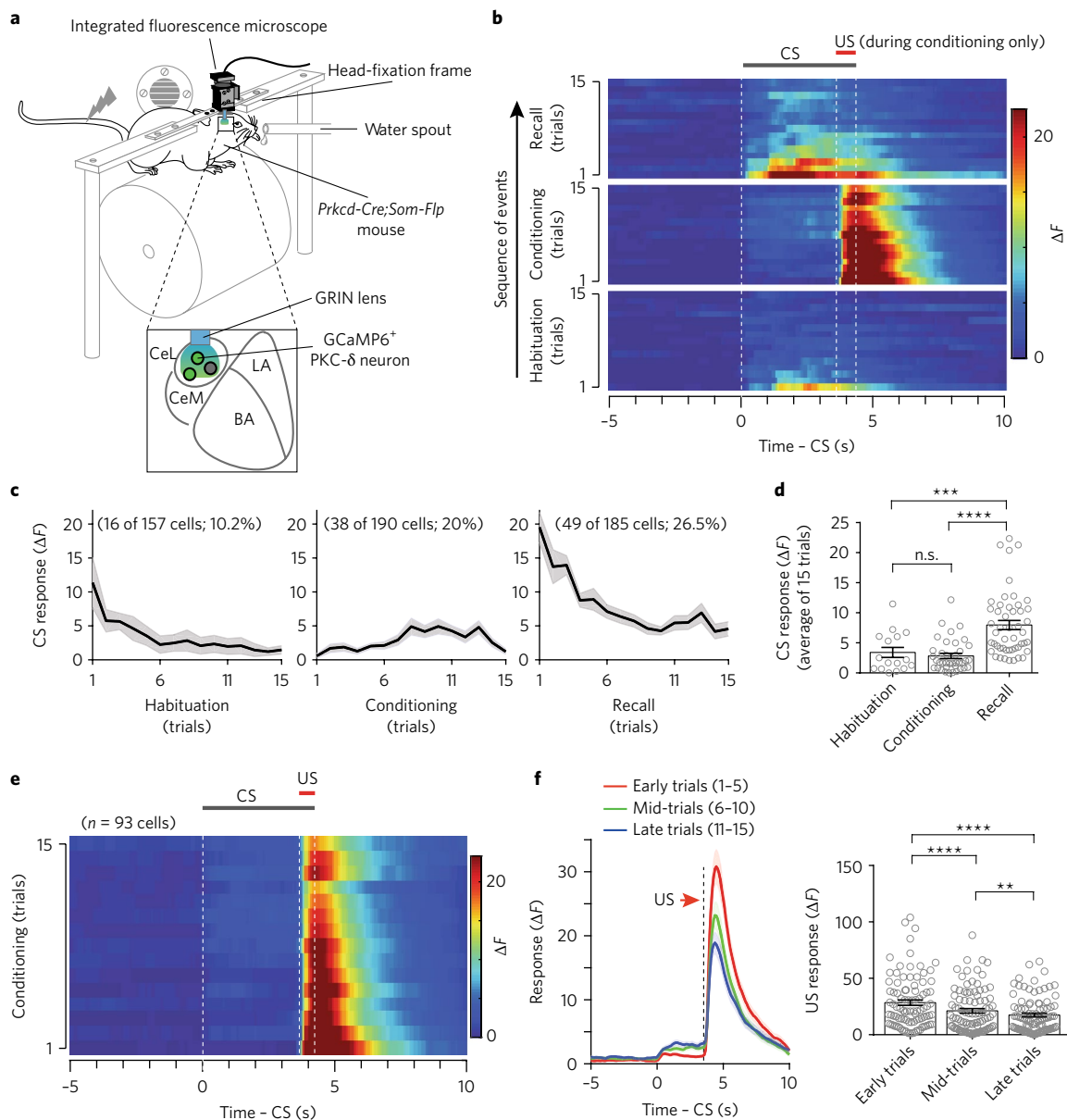


Fig. 2 | CS and US responses in PKC- δ ⁺ CeL neurons during fear conditioning. **a**, A schematic of the experimental configuration. GRIN lens, gradient-index lens. **b**, Heat maps of the average temporal calcium activities of all CS-responsive PKC- δ ⁺ CeL neurons (data from 3 mice) for each trial during habituation, conditioning and recall. Dashed lines indicate the timing of CS or US. **c**, Average CS-induced responses in the same neurons as in **b** for each trial. Shaded areas represent s.e.m. **d**, CS responses of the same neurons as in **c**, averaged for all trials during habituation, conditioning or recall ($F_{2,100} = 17.97$, $P < 0.0001$; $***P < 0.001$, $****P < 0.0001$; n.s., not significant ($P > 0.05$); one-way ANOVA followed by Bonferroni's test). **e**, Heat map of the average temporal calcium activities of all US-responsive PKC- δ ⁺ CeL neurons for each trial during conditioning. Dashed lines indicate the timing of CS or US. **f**, The time course (left) and peak amplitude (right) of US-evoked responses in the same neurons as those in **e**, averaged for the trials in different stages of conditioning ($n = 93$ cells, 3 mice; $F_{1,140.2} = 26.41$, $P < 0.0001$; $**P < 0.01$, $****P < 0.0001$; one-way RM-ANOVA followed by Bonferroni's test; shaded areas in **f** represent s.e.m.). Data are presented as mean \pm s.e.m. in **c**, **d**, and **f**.

As a first step to test this possibility, we performed another optogenetic inhibition experiment, in which we restricted the inhibition of PKC- δ ⁺ CeL neurons to the period of US presentation during conditioning. This manipulation was sufficient to impair the formation of fear memory (Supplementary Fig. 6), supporting a critical role for the PKC- δ ⁺ CeL neurons in processing US.

Next, we examined whether and how PKC- δ ⁺ CeL neurons might respond to US. We delivered GCaMP6, a genetically encoded calcium indicator¹⁵, into PKC- δ ⁺ neurons by injecting the CeL of the *Prkcd-Cre;Som-Flp* mice with an intersectional AAV-C_{on}/F_{off}-GCaMP6m¹⁶. This strategy ensures specific infection of PKC- δ ⁺

neurons and avoids infection of a small fraction of CeL neurons expressing both PKC- δ and SOM². The same mice were implanted in the CeL with gradient-index lenses, through which the calcium signals could be recorded using a miniature integrated fluorescence microscope (Fig. 2a)¹⁷. We subsequently trained these mice in the conditioned lick-suppression task (Supplementary Fig. 4)⁷ while imaging PKC- δ ⁺ CeL neuron calcium responses (Fig. 2a and Supplementary Fig. 7).

We identified active PKC- δ ⁺ CeL neurons based on their spontaneous activities and CS or US responses (see Methods; Supplementary Figs. 7 and 8 and Supplementary Video 1). The fractions of neurons

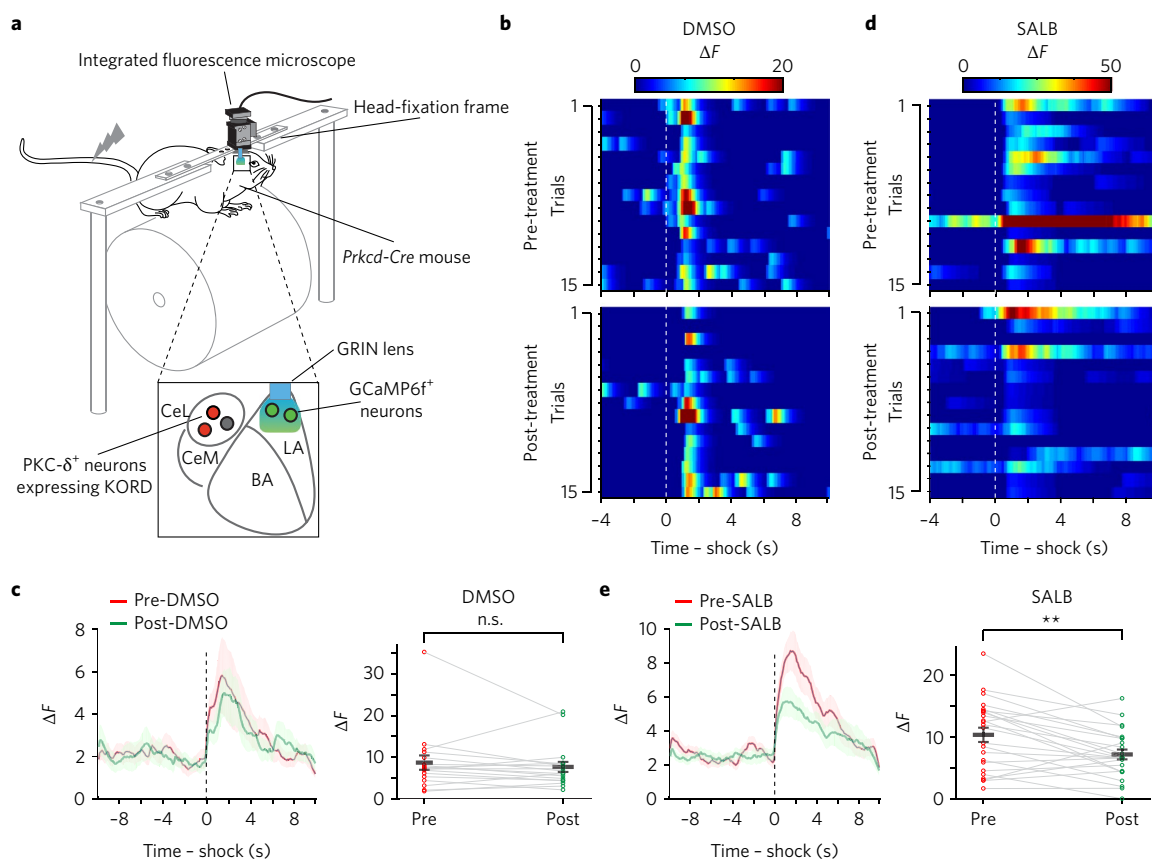


Fig. 3 | PKC- δ^+ CeL neurons are required for the US responses of LA neurons. **a**, A schematic of the experimental configuration. KORD, kappa-opioid receptor. **b**, Heat maps of the temporal calcium activities of a representative LA neuron, before (top) and after (bottom) application of DMSO (dimethyl sulfoxide, an organosulfur solvent). Dashed line indicates the onset of US. **c**, Left: average temporal activities of all shock-responsive LA neurons aligned to shock onset (dashed line), before and after DMSO treatment. Shaded areas represent s.e.m. Right: scatter plot of the peak shock responses of each neuron before and after DMSO treatment ($t_{17} = 0.93$, n.s., $P > 0.05$; paired t test; $n = 18$ neurons from 4 mice; 18 of 123 (15%) of LA neurons showed shock responses). **d,e**, As in **b** and **c**, respectively, except that salvinorin B (SALB, dissolved in DMSO) was applied instead of DMSO alone to the same mice in different imaging sessions ($t_{23} = 3.5$, $**P < 0.01$; paired t test; $n = 24$ neurons from 4 mice; 24 of 143 (17%) of LA neurons showed shock responses). Data are presented as mean \pm s.e.m. in **c** and **e**.

showing CS-evoked responses were 10.2% (16 of 157), 20.0% (38 of 190) and 26.5% (49 of 185) during habituation, conditioning and recall, respectively ($P < 0.05$, χ^2 test with Bonferroni's correction, comparing habituation with other groups; Fig. 2b–d). On average, the CS responses of these neurons desensitized during habituation but recovered quickly following US presentations during conditioning and were enhanced during recall (Fig. 2b–d). These results indicate that PKC- δ^+ CeL neurons acquire CS responses following FC.

During conditioning, 48.9% (93 of 190) of PKC- δ^+ CeL neurons showed prominent US-evoked responses (Fig. 2b,e,f and Supplementary Fig. 8). Notably, these responses decreased as conditioning progressed (Fig. 2b,e,f; 39 of 93 cells (42%) showed significant decrease, $P < 0.05$), consistent with theories and evidence that instructive US signals are suppressed when they become expected^{9,18–20}. To specifically test the effect of expectation, we tracked the responses of each PKC- δ^+ CeL neuron to a series of US presentations, some of which were signaled by the CS while the others were delivered unexpectedly (Supplementary Fig. 9a,b). We found that, among all US-responsive neurons, 21.1% had stronger responses, while 8.8% showed weaker responses to unsignaled than to signaled US (Supplementary Fig. 9b–e). These results demonstrate that about half of PKC- δ^+ CeL neurons show robust US responses, with a sub-population of these neurons having US responses suppressed by expectation, the property of a teaching signal^{9,18–20}.

To examine the role of PKC- δ^+ CeL neurons in conveying the US to the LA, we implanted gradient-index lenses in the LA of *Prkcd-Cre* mice in which the GCaMP6 was expressed in LA neurons and in which an inhibitory DREADD (designer receptor exclusively activated by designer drugs) derived from the kappa-opioid receptor (Supplementary Fig. 10 and Methods) was selectively expressed in PKC- δ^+ CeL neurons (Fig. 3a and Supplementary Fig. 11) by AAVs. This strategy allowed us to track the US responses of the same LA neurons (Supplementary Fig. 12a–e and Supplementary Video 2) before and after transiently inhibiting PKC- δ^+ CeL neurons with systemically applied salvinorin B, a kappa-opioid receptor agonist (Methods and Fig. 3). We found that LA neurons had longer response latencies in response to shocks than PKC- δ^+ CeL neurons (Supplementary Fig. 12f). Notably, inhibition of PKC- δ^+ CeL neurons suppressed shock-evoked responses of LA neurons (Fig. 3b–e). These results indicate that PKC- δ^+ CeL neurons play an important role in conveying US signal to the LA.

If PKC- δ^+ CeL neurons convey US during FC, they may also carry negative emotional valence and, moreover, may be able to instruct learning. Indeed, we found that inhibition of these neurons with the TeLC reduced animals' reactions to electrical shocks (Supplementary Fig. 13a), suggesting that these neurons are important for processing the affective component of

the US. Conversely, optogenetic activation of PKC- δ^+ CeL neurons induced aversion in mice in a real-time place-aversion task (Supplementary Figs. 13b,c and 14a). Furthermore, in a conditioned place-aversion task, pairing optogenetic activation of PKC- δ^+ CeL neurons with one side of a chamber caused mice to avoid that side when tested in the following day (Supplementary Figs. 13d and 14b). Together, these results indicate that PKC- δ^+ CeL neurons convey aversive information and are sufficient to drive aversive learning.

To identify the potential routes through which PKC- δ^+ CeL neurons may convey US information to the LA, we conducted anatomic tracing experiments. We recently developed an anterograde trans-synaptic herpes simplex virus, type 1 strain 129, which expresses four copies of GFP (H129-G4) and is therefore bright enough for direct visualization of labeled neurons (Methods); we injected this into the CeL. This resulted in the labeling of cells in a number of brain regions downstream of CeL neurons (Supplementary Fig. 15). We next specifically infected PKC- δ^+ CeL neurons with an AAV expressing the red fluorescent protein mRuby and screened for areas innervated by axon fibers originating from these neurons (Supplementary Fig. 16). The regions identified by both methods, including the bed nucleus of the stria terminalis (BNST), substantia innominata (SI), central medial amygdaloid nucleus (CeM), substantia nigra pars compacta (SNc), retrorubral field (RRF) and PBN, are the potential postsynaptic targets of PKC- δ^+ CeL neurons (Supplementary Figs. 15 and 16). Finally, using retrograde tracing methods, we revealed that, among these regions, SI, SNc and RRF send direct projections to the basolateral amygdaloid nucleus (BLA; Supplementary Fig. 17a–h) and that most of those BLA-projecting SNc neurons are dopaminergic (Supplementary Fig. 17f–h). Thus, neurons in these areas are good candidates for relaying US information from PKC- δ^+ CeL neurons to the LA. Notably, it has been shown that midbrain dopamine neurons, including those in the SNc (Supplementary Fig. 17f–h), play an important role in fear learning and that CeA neurons preferentially innervate GABAergic neurons over dopaminergic neurons in the SNc and ventral tegmental area (VTA; Supplementary Fig. 18). Therefore, it is likely that PKC- δ^+ CeL neurons drive disinhibition of dopamine neurons in response to US, thereby instructing learning in the LA (Supplementary Fig. 18). Alternatively, or additionally, neurons in the SI or the RRF may also mediate the function of PKC- δ^+ CeL neurons.

Altogether, our results indicate that PKC- δ^+ CeL neurons play an important role in conveying information about US to the LA during FC, hence uncovering a previously unknown amygdala functional organization (Supplementary Fig. 18). Our findings also revise a prevailing model for the function of PKC- δ^+ CeL neurons, which posits that these neurons are ‘fear-off’ neurons (a CeL population that shows inhibitory CS responses following fear conditioning⁸) that act to suppress fear responses through tonic inhibition of amygdala output¹². In fact, we show that a substantial population of PKC- δ^+ CeL neurons are essentially ‘fear-on’ neurons as they convey aversive US signals, drive aversive learning and are activated by the CS predicting the US. Furthermore, optogenetic silencing of PKC- δ^+ CeL neurons did not induce any freezing behavior or aversive responses (Supplementary Fig. 5), which would be expected if these neurons were fear-off neurons¹². Nevertheless, it is still possible that some of the fear-off neurons in the CeL may indeed be PKC- δ^+ neurons that evaded detection in our experiments. It is certainly possible that PKC- δ^+ CeL neurons are heterogeneous, subserving aversive learning (this study), regulation of feeding, and other distinct functions that can be determined, at least in part, by the divergent projections of these neurons (Supplementary Figs. 15 and 16; and see Supplementary Fig. 18) together with the various inputs that they may receive^{2,4,13}.

Methods

Methods, including statements of data availability and any associated accession codes and references, are available at <https://doi.org/10.1038/s41593-017-0009-9>.

Received: 10 April 2017; Accepted: 29 September 2017;

Published online: 23 October 2017

References

- Herry, C. & Johansen, J. P. Encoding of fear learning and memory in distributed neuronal circuits. *Nat. Neurosci.* **17**, 1644–1654 (2014).
- Li, H. et al. Experience-dependent modification of a central amygdala fear circuit. *Nat. Neurosci.* **16**, 332–339 (2013).
- Penzo, M. A., Robert, V. & Li, B. Fear conditioning potentiates synaptic transmission onto long-range projection neurons in the lateral subdivision of central amygdala. *J. Neurosci.* **34**, 2432–2437 (2014).
- Penzo, M. A. et al. The paraventricular thalamus controls a central amygdala fear circuit. *Nature* **519**, 455–459 (2015).
- Goosens, K. A. & Maren, S. Pretraining NMDA receptor blockade in the basolateral complex, but not the central nucleus, of the amygdala prevents savings of conditional fear. *Behav. Neurosci.* **117**, 738–750 (2003).
- Wilensky, A. E., Schafe, G. E., Kristensen, M. P. & LeDoux, J. E. Rethinking the fear circuit: the central nucleus of the amygdala is required for the acquisition, consolidation, and expression of Pavlovian fear conditioning. *J. Neurosci.* **26**, 12387–12396 (2006).
- Yu, K., Garcia da Silva, P., Albeanu, D. F. & Li, B. Central amygdala somatostatin neurons gate passive and active defensive behaviors. *J. Neurosci.* **36**, 6488–6496 (2016).
- Ciocchi, S. et al. Encoding of conditioned fear in central amygdala inhibitory circuits. *Nature* **468**, 277–282 (2010).
- Roesch, M. R., Esber, G. R., Li, J., Daw, N. D. & Schoenbaum, G. Surprise! Neural correlates of Pearce-Hall and Rescorla-Wagner coexist within the brain. *Eur. J. Neurosci.* **35**, 1190–1200 (2012).
- Balleine, B. W. & Killcross, S. Parallel incentive processing: an integrated view of amygdala function. *Trends Neurosci.* **29**, 272–279 (2006).
- Nabavi, S. et al. Engineering a memory with LTD and LTP. *Nature* **511**, 348–352 (2014).
- Haubensak, W. et al. Genetic dissection of an amygdala microcircuit that gates conditioned fear. *Nature* **468**, 270–276 (2010).
- Han, S., Soleiman, M. T., Soden, M. E., Zweifel, L. S. & Palmiter, R. D. Elucidating an affective pain circuit that creates a threat memory. *Cell* **162**, 363–374 (2015).
- Sato, M. et al. The lateral parabrachial nucleus is actively involved in the acquisition of fear memory in mice. *Mol. Brain* **8**, 22 (2015).
- Chen, T. W. et al. Ultrasensitive fluorescent proteins for imaging neuronal activity. *Nature* **499**, 295–300 (2013).
- Fenno, L. E. et al. Targeting cells with single vectors using multiple-feature Boolean logic. *Nat. Methods* **11**, 763–772 (2014).
- Resendez, S. L. et al. Visualization of cortical, subcortical and deep brain neural circuit dynamics during naturalistic mammalian behavior with head-mounted microscopes and chronically implanted lenses. *Nat. Protoc.* **11**, 566–597 (2016).
- Johansen, J. P., Tarpley, J. W., LeDoux, J. E. & Blair, H. T. Neural substrates for expectation-modulated fear learning in the amygdala and periaqueductal gray. *Nat. Neurosci.* **13**, 979–986 (2010).
- McNally, G. P., Johansen, J. P. & Blair, H. T. Placing prediction into the fear circuit. *Trends Neurosci.* **34**, 283–292 (2011).
- Belova, M. A., Paton, J. J., Morrison, S. E. & Salzman, C. D. Expectation modulates neural responses to pleasant and aversive stimuli in primate amygdala. *Neuron* **55**, 970–984 (2007).

Acknowledgements

We thank G.D. Stuber for helping with the in vivo imaging experiments. We thank G.D. Stuber and J. Johansen for critically reading an earlier version of the manuscript, G.-R. Hwang for technical assistance and members of the Li laboratory for helpful discussions. This work was supported by grants from the National Institutes of Health (NIH) (R01MH101214, B.L.), Human Frontier Science Program (RGP0015/2016, B.L.), NARSAD (23169, B.L., and 21227, S.A.), National Natural Science Foundation of China (81428010, B.L. and M.H., and 91432106, M.H.), China Postdoctoral Science Foundation (2016M590316, L.G.), Louis Feil Trust (B.L.), the Stanley Family Foundation (B.L.), Simons Foundation (344904, B.L.) and Wodcroft Foundation (to B.L.).

Author Contributions

K.Y. and B.L. conceived and designed the study. K.Y., S.A., X.Z. and H.S. conducted experiments (X.Z. performed the experiments in which LA neurons were imaged; S.A. and H.S. performed the experiments in which synaptic plasticity in LA neurons was examined; K.Y. conducted most of the remaining experiments). K.Y., X.Z., S.A. and

H.S. analyzed data. C.R., L.F. and K.D. developed the intersectional viral strategy and provided critical reagents. F.Z. and M.-H.L. developed the H129-G4 viral system and performed the anterograde tracing with it. L.G. and M.H. performed imaging with the STPT. P.Z. and L.P. developed and assisted with the imaging analysis methods (CNMF and CNMF-E). B.L. wrote the paper with inputs from all authors.

Competing financial interests

The authors declare no competing financial interests.

Additional information

Supplementary information is available for this paper at <https://doi.org/10.1038/s41593-017-0009-9>.

Reprints and permissions information is available at www.nature.com/reprints.

Correspondence and requests for materials should be addressed to B.L.

Publisher's note: Springer Nature remains neutral with regard to jurisdictional claims in published maps and institutional affiliations.

Methods

Please also see relevant information in the Life Sciences Reporting Summary.

Animals. Before surgery, mice were housed under a 12-h light–dark cycle (7 a.m. to 7 p.m. light) in groups of 2–5 animals, with food and water freely available. Animals with implants were housed singly. All behavioral experiments were performed during the light cycle. The *Som-cre*²¹, *Prkcd-Cre*¹², *Som-Flp*¹, *Ai32* and *Ai35*²², and *lox-stop-lox-H2B*²³ mice have all been described elsewhere. The *Som-Cre* and *Som-Flp* mice were provided by Z.J. Huang (Cold Spring Harbor Laboratory). The *Prkcd-Cre* mice were purchased from the Mutant Mouse Regional Resource Centers (MMRRC) as cryopreserved spermatozoa (source: N. Heintz (The Rockefeller University)). Other mice were purchased from the Jackson Laboratory. All mice were bred onto a C57BL/6J genetic background. The *Prkcd-Cre;Som-Flp* mice were bred by crossing the *Prkcd-Cre* mice with *Som-Flp* mice. Male and female mice 40–60 d of age were used for all the experiments. All procedures involving animals were approved by the Institute Animal Care and Use Committees of Cold Spring Harbor Laboratory and Wuhan Institute of Virology, Chinese Academy of Sciences.

Viral vectors. The AAV-DIO-TeLC-GFP (the AAV expressing the tetanus toxin light chain (TeLC), which blocks neurotransmitter release²⁴ in a Cre-dependent manner; DIO, double-*loxP*-flanked inverse open reading frame), AAV-DIO-GFP, AAV-CAG-ChR2(H134R)-eYFP, AAV-DIO-ArchT-GFP, AAV-DIO-ChR2(H134R)-eYFP and AAV-hSyn-GCaMP6f viruses (all serotype 2/9) were made by the Penn Vector Core (Philadelphia, PA). The AAV-hSyn-DIO-HA-KORD-IRES-mCitrine (2/8) virus was made by the University of North Carolina Vector Core (Chapel Hill, NC). The AAVdj-hSyn-C_{on}/F_{off}-GCaMP6m and AAVdj-hSyn-C_{on}/F_{off}-hChR2-mCherry viruses were made by the Stanford Vector Core (Stanford, CA). The H129-G4 virus was produced at Wuhan Institute of Virology, Chinese Academy of Sciences, as previously described²⁵. The retrograde canine adenovirus expressing Cre recombinase (CAV2-Cre)²⁶ was purchased from Montpellier vector platform (Plateforme de Vectorologie de Montpellier (PVM), Biocampus Montpellier, Montpellier, France). All viruses were stored in aliquots at –80 °C until use. For AAVs, we waited for at least 5 weeks after injection for optimal viral expression; for the H129-G4, we waited for 3 d before examining the tracing results; for the CAV2-Cre, we waited for 4 weeks.

Stereotaxic surgery. Standard surgical procedures were followed for stereotaxic injection²⁴. Briefly, mice were either anesthetized with ketamine (100 mg per kg of body weight) supplemented with dexmedetomidine hydrochloride (0.4 mg per kg) or anesthetized with isoflurane (using 2% at the beginning and 0.5–1% for the rest of the surgery procedure). Mice were positioned in a stereotaxic injection frame and laid on a heating pad maintained at 35 °C. A digital mouse brain atlas was linked to the injection frame to guide the identification and targeting (Angle Two Stereotaxic System, myNeuroLab.com).

Viruses (~0.3 μ L) were delivered with a glass micropipette (tip diameter: ~5 μ m) through a skull window (1–2 mm²) by pressure applications (5–20 psi, 5–20 ms at 0.5 Hz) controlled by a Picospritzer III (General Valve) and a pulse generator (Agilent). The injection was performed using the following stereotaxic coordinates for the CeL: –1.22 mm from bregma, 2.9 mm lateral from the midline and 4.6 mm vertical from skull surface; for the LA: –1.55 mm from bregma, 3.2 mm lateral from the midline and 4.2 mm vertical from skull surface; and for the MGN: –3.16 mm from bregma, 1.90 mm lateral from the midline and 3.20 mm vertical from skull surface.

For the in vivo photostimulation experiments, immediately after viral injection, mice were bilaterally implanted with optical fibers (core diameter: 105 μ m; Thorlabs, catalog number FG105UCA) that were placed above the CeL (coordinates of the fiber tip: –1.22 mm from bregma, 2.9 mm lateral from the midline and 4.3 mm vertical from skull surface). The optical fiber, together with the ferrule (Thorlabs), was secured to the skull with C&B-Metabond Quick adhesive luting cement (Parkell Prod), followed by dental cement (Lang Dental Manufacturing).

For the in vivo imaging experiments, immediately after viral injection, a gradient-index (GRIN) lens (diameter; 500 μ m; length: ~8.4 mm, part ID 130-000152; Inscopix) was implanted 200 μ m above the center of injection.

For animals used in experiments under head fixation, following the above procedures, a small metal bar was mounted on the skull of each mouse, which was used to hold the mouse in the head fixation frame during experiments.

Immunohistochemistry. Immunohistochemistry experiments were performed following standard procedures. Briefly, mice were anesthetized with Euthasol (0.4 mL; Virbac, Fort Worth, Texas, USA) and transcardially perfused with 40 mL of PBS, followed by 40 mL of 4% paraformaldehyde in PBS. Brains were extracted and further fixed in 4% PFA overnight, followed by cryoprotection in a 30% PBS-buffered sucrose solution for 36 h at 4 °C. Coronal sections (40 or 50 μ m thick) were cut using a freezing microtome (Leica SM 2010R, Leica). Sections were first washed in PBS (3 \times 5 min), incubated in PBST (0.3% Triton X-100 in PBS) for 30 min at room temperature (RT, 22–24 °C) and then washed with PBS (3 \times 5 min). Next, sections were blocked in 5% normal goat serum in PBST for 30 min at RT, and then

incubated with primary antibodies overnight at 4 °C. Sections were washed with PBS (5 \times 15 min) and incubated with fluorescent secondary antibodies at RT for 1 h. After washing with PBS (5 \times 15 min), sections were mounted onto slides with Fluoromount-G (Ebioscience, San Diego, California, USA). Images were taken using a LSM 780 laser-scanning confocal microscope (Carl Zeiss, Oberkochen, Germany). The primary antibodies used were mouse anti-PKC- δ (BD Biosciences, NJ, USA, cat. # 610398); rabbit anti-HA-Tag (C29F4, Cell Signaling, Danvers, MA, USA, cat. # 3724S); and rabbit anti-TH (tyrosine hydroxylase; Millipore, Billerica, MA, USA, cat. # AB152). The fluorophore-conjugated secondary antibody used was Alexa Fluor-594 donkey anti-rabbit IgG (H+L) or Alexa Fluor-488 goat anti-rabbit IgG (H+L; Life Technologies, Carlsbad, California, USA; catalog number A21207 or A11008, respectively), depending on the desired fluorescence color. All antibodies used in this study have been validated by previous studies^{22–24,27,28}.

In vitro electrophysiology. To assess the synaptic plasticity in LA neurons induced by auditory FC, we specifically examined the synaptic transmission onto these neurons driven by the auditory thalamus—the medial geniculate nucleus (MGN)—that conveys the conditioned stimulus to the LA. To this end, we used mice in which the MGN was injected with the AAV-CAG-ChR2(H134R)-YFP, so that the MGN–LA pathway could be optogenetically stimulated in acute slices. We performed patch-clamp recording as previously described²⁴. Briefly, 24 h following fear conditioning and immediately after the recall test (or 24 h following habituation for the naive group), mice were anesthetized with isoflurane before they were decapitated; their brains were then dissected out and placed in ice-cold dissection buffer (110 mM choline chloride, 25 mM NaHCO₃, 1.25 mM NaH₂PO₄, 2.5 mM KCl, 0.5 mM CaCl₂, 7.0 mM MgCl₂, 25.0 mM glucose, 11.6 mM ascorbic acid and 3.1 mM pyruvic acid, gassed with 95% O₂ and 5% CO₂). An HM650 Vibrating-blade Microtome (Thermo Fisher Scientific) was then used to cut 300- μ m thick coronal sections that contained the amygdala. These slices were subsequently transferred to a storage chamber that contained oxygenated artificial cerebrospinal fluid (ACSF; 118 mM NaCl, 2.5 mM KCl, 26.2 mM NaHCO₃, 1 mM NaH₂PO₄, 20 mM glucose, 2 mM MgCl₂ and 2 mM CaCl₂, at 34 °C, pH 7.4, gassed with 95% O₂ and 5% CO₂). Following 40 min of recovery, slices were transferred to RT (20–24 °C), where they were continuously bathed in ACSF.

Usually guided whole-cell patch-clamp recordings from LA neurons were obtained with Multiclamp 700B amplifiers and pCLAMP 10 software (Molecular Devices, Sunnyvale, California, USA) and guided using an Olympus BX51 microscope equipped with both transmitted and epifluorescence light sources (Olympus Corporation, Shinjuku, Tokyo, Japan). LA pyramidal neurons were identified for patching. Light stimulation was used to evoke excitatory postsynaptic currents (EPSCs) driven by the ChR2-expressing axons originating from the MGN. The light source was a single-wavelength LED system (λ = 470 nm; CoolLED.com) connected to the epifluorescence port of the Olympus BX51 microscope. Light pulses of 0.2–0.5 ms, triggered by a TTL signal from the Clampex software (Molecular Devices), were used to evoke synaptic transmission. Synaptic responses were low-pass filtered at 1 kHz and recorded at holding potentials of –70 mV (for AMPA-receptor-mediated responses) and +40 mV (for NMDA-receptor-mediated responses). The AMPA/NMDA (A/N) ratio was calculated as the ratio of peak current at –70 mV to the current at 100 ms after light stimulation onset at +40 mV²⁹. Recordings were made in the ACSF with picrotoxin (100 μ M) added. The internal solution contained 115 mM cesium methanesulfonate, 20 mM CsCl, 10 mM HEPES, 2.5 mM MgCl₂, 4 mM Na₂ATP, 0.4 mM Na₂GTP, 10 mM sodium phosphocreatine and 0.6 mM EGTA (pH 7.2). The EPSCs were analyzed using pCLAMP10 software (Molecular Devices).

All cells that met the standard criteria (leak current < 50 pA, access resistance < 30 M Ω , input resistance > 10 \times access resistance) were selected for analysis. We typically recorded up to 6 cells/slice and 2–3 slices/mouse.

Behavioral tasks. *Fear conditioning measuring conditioned freezing.* We followed standard procedures for conventional auditory FC^{2–4}. Briefly, mice were initially handled and habituated to a conditioning cage, which was a mouse test cage (18 cm \times 18 cm \times 30 cm) with an electrifiable floor connected to an H13-15 shock generator (Coulbourn Instruments). The test cage was located inside a sound-attenuated cabinet (H10-24A; Coulbourn Instruments). Before each conditioning session, the test cage was wiped clean with 70% ethanol. During conditioning, the cabinet was illuminated and the mouse's behavior was captured with a monochrome CCD camera (Panasonic WV-BP334) at 3.7 Hz and stored on a personal computer. FreezeFrame software (Coulbourn Instruments) was used to control the delivery of both tones and foot shocks. For habituation, five 4-kHz, 75-dB tones (conditioned stimulus), each of which was 30 s in duration, were delivered at variable intervals. During conditioning, mice received five presentations of the conditioned stimulus, each of which co-terminated with a 2-s, 0.7-mA foot shock (unconditioned stimulus). The recall of fear memory was tested 24 h following conditioning in a novel illuminated context, where mice were exposed to two presentations of unreinforced conditioned stimulus (120-s interstimulus interval). The novel context was a cage with a different shape (22 cm \times 22 cm \times 21 cm) and floor texture than the conditioning cage. Prior to each use, the floor and walls of the cage were wiped clean with 0.5% acetic acid to make the scent distinct from that of the conditioning cage. Freezing responses to the conditioned stimuli were

analyzed with FreezeFrame software (Coulbourn Instruments). The average of the freezing responses to the two conditioned stimuli during recall was used as an index of the conditioned fear.

Fear conditioning measuring conditioned lick suppression. As previously described⁷, water deprivation started 23 h before training. Mice were trained to stay on a movable wheel under head fixation for 30 min in the first day and 10 min daily afterwards. A metal spout was placed in front of animal mouth for water delivery. The spout also served as part of a custom 'lickometer' circuit, which registered a lick event each time a mouse completed the circuit by licking the spout. The lick events were recorded by a computer through custom software written in LabView (National Instruments). Each lick triggered a single opening of a water valve calibrated to deliver 0.3 μ L water. It took mice 4–7 d to achieve stable licking, the criterion for which was 10 min of continuous licking with no gap longer than 10 s.

Mice with stable licking behavior were first subjected to sound habituation sessions (1 session/d for 2 d), during which auditory stimuli were presented through a computer speaker in each trial. Each stimulus was composed of 5 pips of pure tone (8 kHz, 70 dB). Pip duration was 250 ms, and the inter-pip interval was 750 ms. Each of the habituation sessions contained 15 trials with variable intertrial intervals (30–50 s). Twenty-four hours following habituation, mice were conditioned for 15 trials with variable intertrial intervals (30–50 s). In each of these trials, the auditory stimulus (CS) was presented and followed immediately by a tail shock (US; 100 μ A for 500 ms), which was generated from an isolator (ISO-Flex, A.M.P. Instruments LTD, Israel) and delivered through a pair of wires secured to the tail with silicone tubing. The shock was shortened to 50 ms in the imaging experiments to minimize motion artifact.

We used a lick suppression index to quantify animals' performance in this task: lick suppression index = $(L_{\text{PRE}} - L_{\text{CS}}) / (L_{\text{PRE}} + L_{\text{CS}})$, where L_{PRE} is the number of licks in the 5 s period before CS onset and L_{CS} is the number of licks in the 5 s CS period⁷.

Real-time place aversion (RTPA). As previously described²⁷, one side of a custom chamber (23 \times 33 \times 25 cm; made from Plexiglas) was assigned as the stimulation zone, counterbalanced among mice. Mice were placed individually in the middle of the chamber at the onset of the experiment, the duration of which was 20 min. Laser stimulation (5-ms pulses delivered at 5, 10 or 30 Hz) was triggered when mice entered the stimulation zone and lasted until mice exited the stimulation zone. Mice were videotaped with a CCD camera interfaced with Ethovision software (Noldus Information Technologies), which was used to control the laser stimulation and extract behavioral parameters (position, time, distance and velocity).

Conditioned place aversion. The same chamber use for the RTPA test was used for the conditioned place-aversion test. To make the two sides of the chamber distinct from each other, each side was decorated with a unique visual pattern (dotted vs. striped) and scented with a unique odor (cherry vs. blueberry). The test consisted of four sessions per day for four consecutive days. In session 1, the habituation session, mice were individually placed in the center of the chamber and allowed to freely explore both sides. In sessions 2 and 3, the conditioning sessions, the mice received 10 trials of laser stimulation, each consisting of a 10-s train of 30-Hz, 5-ms pulses, in the side of the chamber designated as the stimulation side (counterbalanced among mice). The exit from the stimulation side was blocked during conditioning. In session 4, the recall session, the mice were allowed to freely explore both sides of the chamber. The mice were videotaped in sessions 1 and 4 with a CCD camera interfaced with Ethovision software (Noldus Information Technologies), which was used to control the laser stimulation and extract behavioral parameters (position, time, distance and velocity)²⁷.

In vivo optogenetics. We used the light-gated cation channel channelrhodopsin (ChR2)³⁰ and the light-sensitive proton pump archaerhodopsin (Arch)³¹ for optogenetic activation and inhibition, respectively, of neuronal activities. For bilateral optogenetic stimulation in the CeL in behaving mice, a rotary joint (Doric Lenses, Inc., Quebec, Canada, catalog number FRJ_1 \times 2i_FC-2M3_0.22) was used in the light delivery path, with one end of the rotary joint connected to a laser source (λ = 473 or 532 nm, OEM Laser Systems) and the other end, which has two terminals, to two optical fibers (for bilateral stimulation) through sleeves (Thorlabs). This configuration allows mice carrying fiberoptic implants to move freely during optogenetic stimulation. The stimulation was typically composed of 5-ms, 30-Hz light pulses delivered for various durations, unless otherwise specified. Laser intensity was 10 mW, measured at the end of optical fibers.

In vivo calcium imaging and analysis. We followed a recently described procedure for the in vivo imaging experiments¹⁷. All imaging experiments were conducted on awake, behaving mice under head fixation in a dark, sound-attenuated box. GCaMP6 fluorescence signals were imaged using a miniature integrated fluorescence microscope system (Inscopix, Palo Alto, CA) with GRIN lenses implanted in the target areas (CeL and LA). We imaged PKC- δ^+ CeL neuron activities while subjecting the mice to sound habituation, conditioning and recall sessions in the conditioned lick-suppression task. Each session contained 15 trials,

with random intertrial intervals (10–30 s). The same mice were subsequently used to image PKC- δ^+ CeL responses to signaled and unsignaled shocks. A total of 16 shocks, 8 signaled and 8 unsignaled, were delivered in a randomly interleaved manner. In addition, the assignment of the first shock as signaled or unsignaled was counterbalanced among the mice.

We also imaged LA neuron responses to shocks before and after transient inhibition of PKC- δ^+ CeL neurons using chemogenetics, in which we used an inhibitory DREADD derived from the kappa-opioid receptor (KORD)³² and applied salvinorin B (SALB) subcutaneously (s.c.; 10 mg/kg of body weight) to activate KORD³². As a control experiment, we imaged LA neuron responses to shocks before and after systemic application (s.c.) of DMSO (the vehicle for SALB). Each session contained 15 trials.

For experiments in which PKC- δ^+ CeL neurons were imaged, we installed a baseplate on top of the GRIN lens for each mouse, as described previously¹⁷. Before imaging, the miniature microscope was attached to the baseplate. The microscope was adjusted such that the best dynamic fluorescence signals were at the focal plane, which was subsequently kept constant across imaging sessions. For experiments in which LA neurons were imaged, the microscope was mounted on top of and aligned with the GRIN lens using a custom-adjustable micromanipulator that allows movement in all three axes. The focus of the microscope was adjusted through the micromanipulator to get the best focal plane, as described above.

During imaging, the Data Acquisition Box of an nVista Imaging System (Inscopix, Palo Alto, CA) was triggered by an NI data acquisition device (USB6008, National Instruments, CA). Compressed grayscale images were then recorded with nVistaHDV2 (Inscopix) at 10 frames per second. The analog gain (1 to 5) and LED output power (8% to 30% of the maximum) of the microscope were set to be constant for the same subject across imaging sessions. During imaging, the timestamps of different events, including the trigger signals sent to the microscope, auditory stimuli, electrical shocks and licks, were recorded with custom software written in LabView (National Instruments, CA).

For imaging data processing and analysis, we began by importing the compressed video files into Mosaic (version 1.0.0b; Inscopix, Palo Alto, CA), in which we trimmed the first frame of the video for each trial to minimize the influence of the flash associated with LED light onset. We subsequently used Mosaic to combine all the trimmed video files into a single TIFF stack, apply a 4-pixel bin to the stack and correct the motion artifact. A new TIFF stack was then saved for further processing.

Next, to address the problem of high levels of background fluorescence intrinsic to one-photon imaging, we applied our newly developed imaging analysis method, extended constrained non-negative matrix factorization (CNMF-E)³³, in which we model the background with two realistic components: one models the constant baseline of each pixel, while the other models fluctuations from out-of-focus signals and is therefore constrained to have low spatial-frequency structure. This decomposition avoids cellular signals being absorbed into the background term. After subtracting the background approximated with this model, we used constrained non-negative matrix factorization (CNMF)³⁴ to demix neural signals and get their denoised and deconvolved temporal activity, termed ΔF .

Data availability. The data that support the findings of this study are available from the corresponding author upon reasonable request.

Code availability. We performed CNMF-E using a custom Matlab algorithm (for a detailed description and availability of this methods, see Zhou et al.³³).

Once the temporal activity of the neurons was extracted, we characterized the CS (sound) or US (shock) responses of each neuron using auROC (area under the receiver–operating characteristic curve) analysis, in which we compared the average ΔF value during the baseline period (2 s immediately before the delivery of CS or US) with that during CS or US presentations (2 s immediately after the onset of CS or US) in each trial by moving a criterion from zero to the maximum ΔF value. We then plotted the probability that the ΔF values during CS or US presentations were greater than the criteria against the probability that the baseline ΔF values were greater than the criteria. The area under this curve quantifies the degree of overlap between the two ΔF distributions (i.e., the discriminability of the two). A permutation test (iterated 5,000 times) was used to determine whether the average ΔF values during CS or US presentations were significantly ($P < 0.05$) higher than during baseline and thus classify a neuron as being CS-responsive or US-responsive, respectively. The peak CS or US response amplitude in each trial was determined by searching the maximum value within a 3.75- or 5-s window, respectively, immediately after stimulus onset.

Anterograde trans-synaptic tracing with H129-G4 and serial two-photon tomography (STPT). H129-G4 viral injection and brain sample preparation were performed at Wuhan Institute of Virology, Chinese Academy of Sciences. STPT imaging was performed at Fudan University. Mice were transcardially perfused with saline and 4% paraformaldehyde (PFA) 3 d after injecting the CeL with the H129-G4. The brains were further fixed in 4% PFA at 4 °C overnight, followed by 2–4 d in 0.1 M phosphate buffer (PB) with 30% sucrose at 4 °C for dehydration.

The brains were subsequently stored in PB at -20°C until imaging. Detailed information about STPT imaging and related analysis procedures has been described previously^{35,36}. Briefly, the brain was embedded in 4% oxidized agarose and cross-linked by sodium borohydride. The embedded brain was placed on the motorized stage in a Tissuecyte 1000 (Tissuevision) and the whole brain was imaged at a resolution of $1\ \mu\text{m}$ at the x,y plane for a series of 280 z -sections, with $50\text{-}\mu\text{m}$ intersection intervals. The signals from the green channel (GFP signal) and from the red channel (background) were simultaneously acquired, and the latter was used to subtract background from the green channel to enhance the signal to noise ratio.

Retrograde tracing. For retrograde tracing, CAV2-Cre ($\sim 0.25\ \mu\text{L}$) or cholera toxin subunit B (CTB; $\sim 0.1\ \mu\text{L}$) was injected into the LA of *lox-stop-lox-H2B* or wild-type mice, respectively. We waited 4 weeks (for CAV2-Cre) or 1 week (for CTB) after injections before examining the tracing results.

Statistics and data presentation. All statistical tests are indicated where used. Statistical analyses were performed in Origin8 software (OriginLab Corporation, Northampton, MA), GraphPad Prism (GraphPad Software, Inc., La Jolla, CA) or Matlab (MathWorks, Natick, MA). No statistical methods were used to predetermine sample sizes, but our sample sizes are similar to those reported in previous publications^{2–4,7}. Normality was tested by D'Agostino-Pearson or Shapiro-Wilk normality tests. All tests are two-sided. No randomization was used to assign experimental groups, but mice were assigned to specific experimental groups without bias. Data collection and analysis were not performed blind to the conditions of the experiments. All experiments were controlled by computer systems, and data were collected and analyzed in an automated and unbiased way. No mice or data points were excluded.

References

21. Taniguchi, H. et al. A resource of Cre driver lines for genetic targeting of GABAergic neurons in cerebral cortex. *Neuron* **71**, 995–1013 (2011).
22. Madisen, L. et al. A toolbox of Cre-dependent optogenetic transgenic mice for light-induced activation and silencing. *Nat. Neurosci.* **15**, 793–802 (2012).
23. He, M. et al. Cell-type-based analysis of microRNA profiles in the mouse brain. *Neuron* **73**, 35–48 (2012).
24. Murray, A. J. et al. Parvalbumin-positive CA1 interneurons are required for spatial working but not for reference memory. *Nat. Neurosci.* **14**, 297–299 (2011).
25. Zeng, W. B. et al. Anterograde monosynaptic transneuronal tracers derived from herpes simplex virus 1 strain H129. *Mol. Neurodegener.* **12**, 38 (2017).
26. Bru, T., Salinas, S. & Kremer, E. J. An update on canine adenovirus type 2 and its vectors. *Viruses* **2**, 2134–2153 (2010).
27. Stephenson-Jones, M. et al. A basal ganglia circuit for evaluating action outcomes. *Nature* **539**, 289–293 (2016).
28. Beier, K. T. et al. Circuit architecture of VTA dopamine neurons revealed by systematic input-output mapping. *Cell* **162**, 622–634 (2015).
29. Clem, R. L. & Huganir, R. L. Calcium-permeable AMPA receptor dynamics mediate fear memory erasure. *Science* **330**, 1108–1112 (2010).
30. Zhang, F., Wang, L. P., Boyden, E. S. & Deisseroth, K. Channelrhodopsin-2 and optical control of excitable cells. *Nat. Methods* **3**, 785–792 (2006).
31. Chow, B. Y. et al. High-performance genetically targetable optical neural silencing by light-driven proton pumps. *Nature* **463**, 98–102 (2010).
32. Vardy, E. et al. A new DREADD facilitates the multiplexed chemogenetic interrogation of behavior. *Neuron* **86**, 936–946 (2015).
33. Zhou, P. et al. Efficient and accurate extraction of in vivo calcium signals from microendoscopic video data. Preprint at <https://arxiv.org/abs/1605.07266> (2016).
34. Pnevmatikakis, E. A. et al. Simultaneous denoising, deconvolution, and demixing of calcium imaging data. *Neuron* **89**, 285–299 (2016).
35. Ragan, T. et al. Serial two-photon tomography for automated ex vivo mouse brain imaging. *Nat. Methods* **9**, 255–258 (2012).
36. Kim, Y. et al. Whole-brain mapping of neuronal activity in the learned helplessness model of depression. *Front. Neural Circuits* **10**, 3 (2016).

Life Sciences Reporting Summary

Nature Research wishes to improve the reproducibility of the work that we publish. This form is intended for publication with all accepted life science papers and provides structure for consistency and transparency in reporting. Every life science submission will use this form; some list items might not apply to an individual manuscript, but all fields must be completed for clarity.

For further information on the points included in this form, see [Reporting Life Sciences Research](#). For further information on Nature Research policies, including our [data availability policy](#), see [Authors & Referees](#) and the [Editorial Policy Checklist](#).

► Experimental design

1. Sample size

Describe how sample size was determined.

No statistical methods were used to pre-determine sample sizes but our sample sizes are similar to those reported in previous publications (e.g., Li et al., 2013, Nature Neuroscience; Penzo et al., 2015, Nature; Yu et al., 2016, The Journal of Neuroscience).

2. Data exclusions

Describe any data exclusions.

No data points were excluded.

3. Replication

Describe whether the experimental findings were reliably reproduced.

Yes; all attempts at replication were successful

4. Randomization

Describe how samples/organisms/participants were allocated into experimental groups.

No randomization was used to assign experimental groups, but mice were assigned to specific experimental groups without bias.

5. Blinding

Describe whether the investigators were blinded to group allocation during data collection and/or analysis.

Behavioral tests and electrophysiological data acquisition were performed by an investigator with knowledge of the identity of the experimental groups. All behavior experiments were controlled by computer systems, and data were collected and analyzed in an automated and unbiased way.

Note: all studies involving animals and/or human research participants must disclose whether blinding and randomization were used.

6. Statistical parameters

For all figures and tables that use statistical methods, confirm that the following items are present in relevant figure legends (or in the Methods section if additional space is needed).

- | | |
|--------------------------|--|
| n/a | Confirmed |
| <input type="checkbox"/> | <input checked="" type="checkbox"/> The <u>exact sample size</u> (n) for each experimental group/condition, given as a discrete number and unit of measurement (animals, litters, cultures, etc.) |
| <input type="checkbox"/> | <input checked="" type="checkbox"/> A description of how samples were collected, noting whether measurements were taken from distinct samples or whether the same sample was measured repeatedly |
| <input type="checkbox"/> | <input checked="" type="checkbox"/> A statement indicating how many times each experiment was replicated |
| <input type="checkbox"/> | <input checked="" type="checkbox"/> The statistical test(s) used and whether they are one- or two-sided (note: only common tests should be described solely by name; more complex techniques should be described in the Methods section) |
| <input type="checkbox"/> | <input checked="" type="checkbox"/> A description of any assumptions or corrections, such as an adjustment for multiple comparisons |
| <input type="checkbox"/> | <input checked="" type="checkbox"/> The test results (e.g. P values) given as exact values whenever possible and with confidence intervals noted |
| <input type="checkbox"/> | <input checked="" type="checkbox"/> A clear description of statistics including <u>central tendency</u> (e.g. median, mean) and <u>variation</u> (e.g. standard deviation, interquartile range) |
| <input type="checkbox"/> | <input checked="" type="checkbox"/> Clearly defined error bars |

See the web collection on [statistics for biologists](#) for further resources and guidance.

► Software

Policy information about [availability of computer code](#)

7. Software

Describe the software used to analyze the data in this study.

Ethovision XT 5.1 (Noldus Information Technologies)
pCLAMP 10.2 (Molecular Devices, Sunnyvale, California, USA)
ImageJ 1.43 (NIH)
GraphPad Prism 7 (GraphPad Software, Inc., La Jolla, CA).
Origin8 Software (OriginLab Corporation, Northampton, MA).
Mosaic (version 1.0.0b; Inscopix, Palo Alto, CA).
Matlab (MathWorks, Natick, MA)
Matlab algorithm for the CNMF-E method

For manuscripts utilizing custom algorithms or software that are central to the paper but not yet described in the published literature, software must be made available to editors and reviewers upon request. We strongly encourage code deposition in a community repository (e.g. GitHub). *Nature Methods* [guidance for providing algorithms and software for publication](#) provides further information on this topic.

► Materials and reagents

Policy information about [availability of materials](#)

8. Materials availability

Indicate whether there are restrictions on availability of unique materials or if these materials are only available for distribution by a for-profit company.

All materials used are readily available from the authors or from standard commercial sources, which were specified in the Methods section.

9. Antibodies

Describe the antibodies used and how they were validated for use in the system under study (i.e. assay and species).

The primary antibodies used were: mouse anti-PKC- δ (BD Biosciences, NJ, USA, cat. # 610397); rabbit anti-HA-Tag (C29F4, Cell Signaling, Danvers, MA, USA, cat. # 3724S); rabbit anti-TH (tyrosine hydroxylase) antibody (Millipore, Billerica, MA, USA, cat. # AB152).
The fluorophore-conjugated secondary antibody used was Alexa Fluor® 594 donkey anti-rabbit IgG (H+L) or Alexa Fluor® 488 goat anti-rabbit IgG (H+L) (Life Technologies, Carlsbad, California, USA; catalogue number A21207 or A11008, respectively).
They have all been extensively validated by many labs in the world, using transgenic and reporter mice (as positive controls), with Western blot or immunohistochemistry techniques, etc.

10. Eukaryotic cell lines

a. State the source of each eukaryotic cell line used.

No eukaryotic cell lines were used.

b. Describe the method of cell line authentication used.

No eukaryotic cell lines were used.

c. Report whether the cell lines were tested for mycoplasma contamination.

No eukaryotic cell lines were used.

d. If any of the cell lines used are listed in the database of commonly misidentified cell lines maintained by [ICLAC](#), provide a scientific rationale for their use.

No misidentified cell lines were used.

► Animals and human research participants

Policy information about [studies involving animals](#); when reporting animal research, follow the [ARRIVE guidelines](#)

11. Description of research animals

Provide details on animals and/or animal-derived materials used in the study.

Mice:

The following mice are available at the Jackson Laboratory, Bar Harbor, Maine, USA:

Som-cre (stock #013044); Som-Flp (stock #028579); Ai14 (stock #007914); Ai32 (stock #012569); and Ai35 (stock #012735).

The lox-stop-lox-H2B mice were provided by J. Z. Huang at CSHL.

The Prkcd-Cre mice were purchased from the Mutant Mouse Regional Resource Centers (MMRRC) as cryo-preserved spermatozoa (Donor: Dr. Nathaniel Heintz).

Mice of 40–60 d of age were used for all the experiments. Both male and female mice were used in most experiments, in which the data were pooled as no gender difference was observed. The information is provided in the Methods section.

Policy information about [studies involving human research participants](#)

12. Description of human research participants

Describe the covariate-relevant population characteristics of the human research participants.

The study did not involve human research participants.